Adv. Sci. Res., 4, 83–88, 2010
www.adv-sci-res.net/4/83/2010/
doi:10.5194/asr-4-83-2010

Advances in Science & Research
Open Access Proceedings

WRF model and ASAR-retrieved 10 m wind field comparison in a case study over Eastern Mediterranean Sea

M. M. Miglietta, S. Zecchetto, and F. De Biasio

Institute of Atmospheric Sciences and Climate, Italian National Research Council (ISAC-CNR), Section of Padova, Italy

Received: 8 April 2010 – Revised: 11 June 2010 – Accepted: 25 June 2010 – Published: 1 July 2010

Abstract. In Synthetic Aperture Radar (SAR) imagery, signatures of coherent atmospheric structures, due to sea surface roughness modulation by surface winds, are usually well detected. In the present study, the wind field derived from the Envisat Advanced SAR (ASAR) sensor has been analyzed and compared with those simulated with a regional atmospheric model in a case study over an area located in the eastern Mediterranean Sea, extending southward and eastward of Crete island. This is a region subject to complex wind patterns, due to the interaction of the almost steady northerly Etesian wind with the orography of the islands in the region.

The ASAR Wide Swath Mode images provide datasets at resolutions exceptionally high compared to model data, appropriate for investigating the mesoscale phenomena on the marine atmospheric boundary layer and to retrieve the surface wind field. The latter has been obtained with a methodology based on the 2-D Continuous Wavelet Transform, suitable to isolate the backscatter patterns on the base of energy and scale considerations.

Numerical simulations with the Weather Research and Forecasting (WRF) model have been performed using three 2-way nested domains, the inner one covering the area of interest with a resolution of 1 km. Several simulations, using different diffusion and boundary layer parameterization schemes, have been performed in a case study corresponding to mountain lee waves detected in the ASAR image. The 10 m winds resulting from the numerical experiments have been compared to those retrieved from the ASAR, both quantitatively and qualitatively, in order to analyze the correspondence of observed and simulated wind structures.

1 Introduction

The spatial and temporal scales typical of the atmosphere-ocean interaction range from the micro-scale (O(1) m, O(1) s) to the synoptic scale (O(1000) km, O(10) days). While the interaction processes at synoptic scale are fairly well known, those at meso-β and meso-γ scales, relative respectively to atmospheric processes from 20 km to 200 km and from 2 km to 20 km (Orlanski, 1975) are still to be fully understood, as the amount of available data is generally insufficient to completely resolve these scales and the representation of sub-grid processes in the parametrization schemes of the atmospheric models is only approximated.

Significant modulations of the wind field may occur locally, especially in regions of surrounding steep orography. For example, when a fluid element is displaced vertically by mountains, gravity tries to restore the parcel toward equilibrium resulting in an oscillation called gravity wave. Stationary gravity waves on the downstream side of an obstacle are called lee waves (see Smith, 1979; Atkinson, 1981). As wind field leaves imprints at the sea surface detectable by radars, the presence of atmospheric waves can be identified by such sensors. Satellite-borne scatterometers are able to measure the wind blowing inside the marine atmospheric boundary layer, providing information about the spatial structure of the wind in the marine surface layer over large areas. However, they have a resolution too coarse for coastal applications, where the wind needs to be determined as close to the coast as possible. Thus, at present, the Synthetic Aperture Radar

Correspondence to: M. M. Miglietta (m.miglietta@isac.cnr.it)

Published by Copernicus Publications.

(SAR), due to its very fine spatial resolution, is the appropriate sensor for a spatial high resolution wind determination (see Zecchetto and De Biasio, 2008 and the references quoted hereafter).

Global models cannot simulate accurately the strength and the spatial pattern of the winds in regional basins in the lowest levels. This is mainly a consequence of the wavenumber truncation of the spectral resolution of these models, corresponding in the best cases to some tens of km. Such a low resolution prevents from the detailed representation of the coastal morphology (and, in particular, of the land orography), and from the explicit representation of important processes, such as turbulence, convection, ..., that thus need to be parameterized. The task of simulating the weather fields with better local accuracy is usually pursued by using limited area models, which integrate the model equations only on limited geographical domains, but with finer horizontal resolution. The application of these models permits to better represent the small scale forcings, e.g. topographic features, and the internal dynamics and physics, so that a consistent downscaling of the large scale forecasts is produced. This is particularly relevant for those fields with low spatial correlation, such as precipitation, or strongly related to local terrain features, as the 10 m wind field.

The generation of gravity waves and the sheltering effects due to interaction of intense winds with the orography have been studied theoretically (Scorer and Wilkinson, 1956; Gjevik and Marthinsen, 1978) and are well documented from satellite imagery in the literature (Thomson et al, 1992; Vachon et al., 1994; Vachon et al., 1995). In the present paper, intense atmospheric lee waves downwind Crete and Rhodos have been analyzed. The 10 m wind fields simulated with the Weather Research and Forecasting (WRF) atmospheric model (Skamarock et al., 2005) are compared with the sea surface winds derived from an Envisat ASAR wide swath image, obtained using the two-dimensional Continuous Wavelet Transform (2D-CWT) analysis. The purpose of the paper is to test the ability of the WRF model to reproduce the features shown in the ASAR data and to identify a model configuration optimal for wind field simulation. The methodology used for the retrieval of wind from the ASAR is outlined in Sect. 2; in Sect. 3, the model implementation is briefly presented; in Sect. 4, the wind patterns obtained in simulations with different parameterization schemes and different treatments of diffusion are compared to each other and with the ASAR retrieved wind fields. Conclusions are given in Sect. 5.

2 ASAR

The satellite image used here (Fig. 1) is an Envisat ASAR Wide Swath Mode image in VV polarization (ESA, 2002). It covers an area of about 400 km by 400 km (with pixel size of 75 m by 75 m) in the Aegean Sea, close to Crete and Rhodos islands, at 08:20 UTC, 15 May 2008. The methodology of wind extraction, explained in detail in Zecchetto and De Biasio (2002, 2008), is able to extract the radar backscatter signatures related to the wind field, from which it is possible to derive the de-aliased wind direction. With the wind direction information, it is possible to evaluate the wind speed from the CMOD-5 model developed for C-band scatterometers (Hersbach et al., 2007). This model requires the knowledge of the radar incidence angle, of the normalized radar cross section and of the angle between the radar looking and the wind direction. Since the wind directions are retrieved from the backscatter signatures detected by the analysis, which are more structured and dense when the wind speed is high, the spatial resolution of the resulting wind field depends on the wind speed regime.

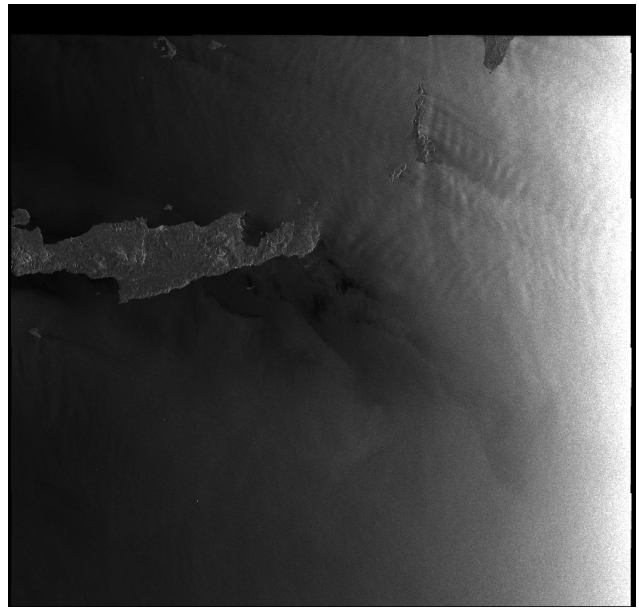

Figure 1. Detail of the Envisat ASAR Wide Swath image at 08:20 UTC, 15 May 2008 in the vicinity of Crete. Pixel size is 75 m by 75 m.

3 WRF model

In the present study, the Weather Research and Forecasting (WRF) model (see http://www.wrf-model.org) has been implemented. For the present study, the model version 3.0 has been implemented in a 3 grid configuration: the largest domain, with a horizontal resolution of 16 km, covers approximately the eastern Mediterranean basin (109×109 grid points); the middle domain covers the area of the Mediterranean sea around Crete with a horizontal resolution of 4 km (161×161 grid points); the inner domain, with a horizontal resolution $\Delta x = \Delta y = 1$ km (321×321 grid points), covers the area (33.6° N–36.4° N, 25° E–28.4° E), that corresponds approximately to the eastern part of Crete, Rhodos island

and the surrounding seas. The coarser grid reproduces the large scale features which force the local dynamics in grid 3, while the intermediate grid is needed as grid 1 and grid 3 have too different horizontal resolutions to be nested directly one into the other. The simulations, starting at 12:00 UTC, 14 May 2008 and lasting 24 h, are performed using a two-way nesting technique. Forty vertical levels are employed, more closely distributed in the lower levels. Initial and boundary conditions every three hours are provided respectively with the European Center for Medium range Weather Forecast (ECMWF) analysis and forecasts. Thus the runs are performed in an operational-like configuration.

A full set of parameterization schemes is included in the model for microphysics, convection, turbulence, soil processes, boundary layer processes, and radiation. In the model configuration used here, the following parameterization schemes have been selected: the Thompson et al. (2004) microphysics, which includes six classes of moisture species plus ice crystal number concentration as prognostic variables; the Kain (2004) cumulus parameterization on the coarser grid (no parameterization is used on the two inner grids); the Rapid Radiative Transfer Model (RRTM) for longwave radiation, based on Mlawer et al. (1997); the Dudhia (1989) scheme for shortwave radiation; a five-layer thermal-diffusion soil scheme (Skamarock et al., 2005). Two different parameterization schemes have been used for the planetary boundary layer (PBL): the Yonsei University (YSU) scheme with a nonlocal turbulent mixing coefficient in the PBL (Hong and Pan, 1996); the Mellor-Yamada-Janjic (MYJ) prognostic scheme that calculates the turbulent kinetic energy (Janjic, 2001).

4 Model versus ASAR wind

The case study is characterized by intense wind impinging on Crete and on nearby islands in the eastern Mediterranean Sea. Such a region is subject to complex wind patterns, due to the interaction of the almost steady northerly Etesian wind with the orography (Koletsis et al., 2009). In order to compare fields with different spatial sampling, both WRF and ASAR-derived winds have been re-sampled on a $0.02^\circ \times 0.02^\circ$ geographical grid, chosen because it permits to preserve the spatial features of both the SAR derived wind (resolution of about 0.001°) and the WRF model (resolution of about 0.01°). The SAR and model-derived wind-vector fields can then be cross-validated, obtaining information on the spatial extent and variability of wind features, and in particular of the atmospheric gravity wave patterns, frequently observed in the region.

The correspondence of the observed with the simulated wind structures has been analyzed for different WRF model simulations performed using two different PBL parameterization schemes (YSU vs. MYJ) and, only for the YSU scheme, different treatments of diffusion. Really, adequate modeling of atmospheric flow features of O(1 km) using limited area models with comparable horizontal grid spacings suffers from the fact that these features are within the maximum energy-containing spectral interval, and they are neither explicitly resolved on the grid nor represented statistically as subgrid motions. We are close to the "no man's land" separating classical Planetary Boundary Layer (PBL) from Large Eddy Simulation (Weisman et al., 2005) schemes. As a result, the ability of mesoscale models to accurately reproduce atmospheric phenomena on such fine spatial scales is questionable, particularly in terms of near-surface flow parameters (Gibbs and Fedorovich, 2009). At the moment, classical PBL schemes are generally employed for grid scales larger than 1 km, although there is no consensus on how to best configure the WRF for these scales (van der Velde et al., 2009; Loughner et al., 2009; Green, 2009; see also http://forum.wrfforum.com).

Figure 2 shows the wind field reproduced by the WRF model using: (a) the YSU scheme without explicit diffusion (hereafter CTL run)[1], (b) the YSU scheme with a second order diffusion based on constant eddy viscosities evaluated on model coordinate surfaces (constant coefficients $k_x = k_y = \Delta x$; hereafter DIFF run), (c) the YSU scheme with a horizontal "Smagorinsky" closure (Smagorinsky, 1963; hereafter SMG run) and finally (d) the MYJ scheme without diffusion (hereafter MYJ run). By comparing Fig. 2a with Fig. 2b, we see that the small-scale details of the wind pattern are progressively lost when larger diffusion coefficients are used.

Figure 2a, c and d shows similar gravity wave structures on the east side, generated by the flow impinging on Rhodos, Crete and the small islands of Kassos and Karpathos in between. The interaction of the wave trains at the lee side of the different islands yields a complex interference pattern, extending more than 80 km downstream. The simultaneous presence of orographic gravity waves and a low-speed island wake southward of Crete suggests that different Froude number regimes occur (Smith, 1989), depending on the local orographic features the wind impinges on.

Some relevant differences among the simulations can be identified close to Crete on the west side of the figure, especially downstream, as local wind maxima occur close to the island in Fig. 2c, d, while they are much more confined in Fig. 2a and missing in Fig. 2b. These maxima are associated with gap flows (Koletsis, 2009) or low level vortices generated downstream (Smolarkiewicz and Rotunno, 1989). Since the structure of the atmospheric boundary layer flow is more complex at the land-sea transition zone, due to the formation of coherent mesoscale circulation triggered by abrupt changes in the surface roughness, thermal forcing, land use, or orography, it is expected that the strongest differences

[1]WRF model includes an implicit scale-selective filter for advection, thus the model can run stably without artificial diffusion; however, it may sometimes be insufficient to remove noise.

Table 1. Bias (WRF-ASAR), standard deviation σ and correlation coefficients R of wind speed (ws) and direction (wd) for the different experiments after resampling at 0.05° by 0.05°. Section 4 explains the characteristics of the different experiments.

Exp.	$bias_{ws}$ (m s^{-1})	$bias_{wd}$ (°)	σ_{ws} (m s^{-1})	σ_{wd} (°)	R_{ws}	R_{wd}
CTL	−0.4	−10	1.9	27	0.6	0.5
SMG	−0.9	−4	2.3	33	0.3	0.3
MYJ	−0.9	−2	2.3	38	0.4	0.3

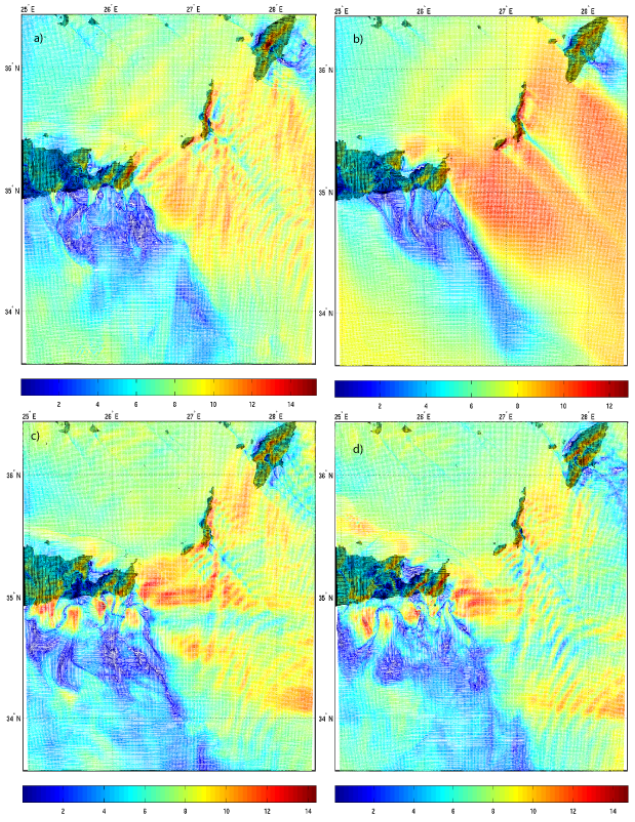

Figure 2. 10 m wind speed (colors) simulated by the WRF model (inner domain) in the CTL run (**a**, left top), the DIFF run (**b**, right top), the SMG run (**c**, left bottom), and the MYJ run (**d**, right bottom) at 08:00 UTC, 15 May 2008. The dark regions correspond to the island location. The maps cover the area delimited with the black border in Fig. 3. Section 4 explains the characteristics of the different experiments.

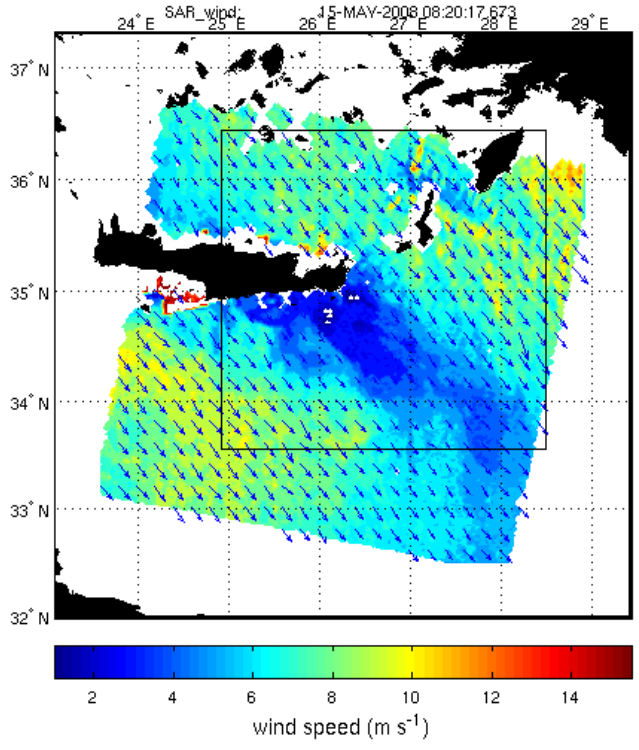

Figure 3. ASAR derived sea surface wind field (speed: colors; direction: arrows) at 08:20 UTC, 15 May 2008. The position of the WRF inner domain is represented with the black border.

among the parameterization schemes may occur in this region (Sood and Bange, 2009).

The ASAR derived wind, derived from the wind direction interpolated on a 0.02° by 0.02° grid, is shown in Fig. 3. The wind direction has been reported with a resolution ten times coarser than the original. The signature of the atmospheric gravity waves is still present. Comparing it with the WRF model fields, a closer resemblance occurs with the CTL run (Fig. 2a) and with the DIFF run (Fig. 2b) in the west side, as the low speed wake downstream of Crete is more uniform, without local wind maxima. In the east side of the domain, all simulations exhibit a wave pattern similar to ASAR, apart from the DIFF experiment, that completely misses the gravity wave structure; as a consequence, this simulation is no longer considered in the following discussion.

In order to provide a more quantitative comparison, the bias, the standard deviation and the correlation coefficients for wind speed and direction between the model simulations and the ASAR data have been calculated. Table 1 shows that the CTL run is the closest to the ASAR data for all the parameters, apart from the wind direction bias.

Figure 4 compares the normalized frequency distributions of wind speed and direction for the CTL run and the ASAR data; for a more comprehensive analysis, also the

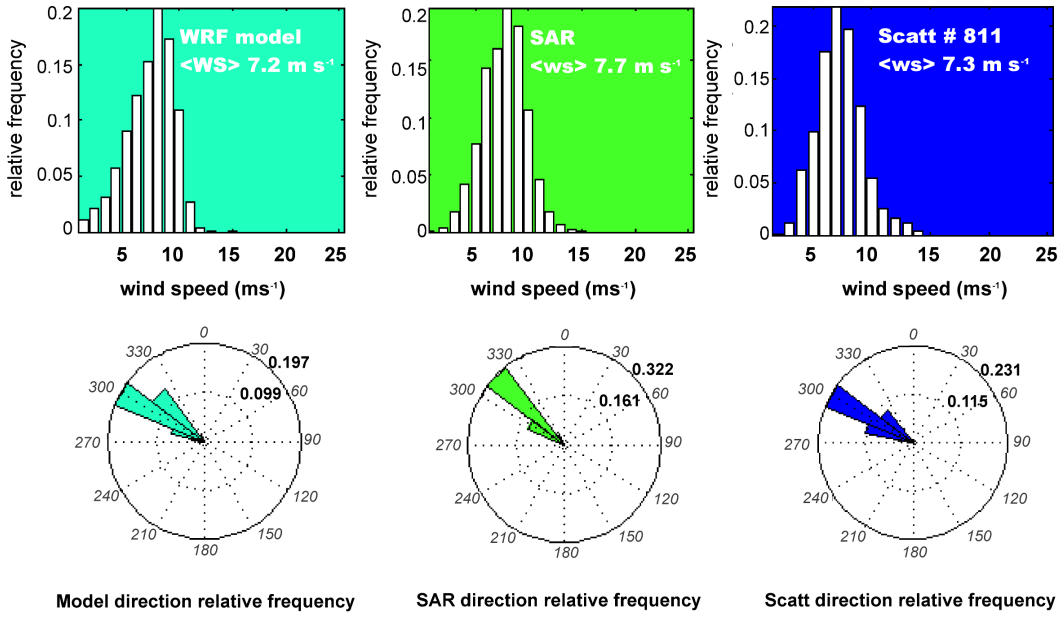

Figure 4. Frequency distributions of wind speeds (top) and wind directions (bottom) from WRF (left), ASAR (middle) and QuikSCAT (right) after resampling at 0.05° by 0.05°.

distributions obtained from the scatterometer winds derived from the NASA QuikSCAT satellite (JPL, 2006) are shown. The three patterns appear similar; however, a shift of the model distribution toward lower speeds and a threshold of 12 m s^{-1}, not present in ASAR and QuikSCAT winds, can be identified. About the direction, a prevailing NW component is present in all cases, although the distribution is less unidirectional and slightly rotated anticlockwise for the WRF model and the scatterometer.

Figure 5 shows a wind speed scatterplot for the CTL run and the ASAR data, with the colors indicating the frequency of wind speed in given bins of 1 m s^{-1}; it indicates a pretty good agreement between the two datasets. Again, the figure shows a general underestimation by the model, that is mainly due to the winds in the south-west side of the domain, where the model is not able to reproduce the relative maximum.

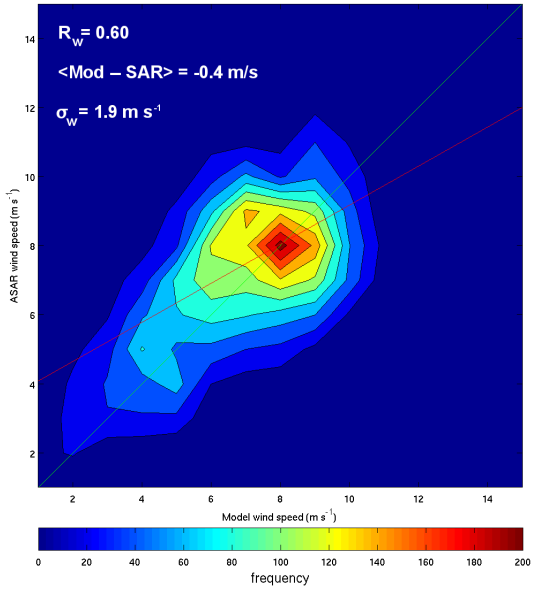

Figure 5. Scatterplot between the CTL run and the ASAR data after resampling at 0.05° by 0.05°. Colors indicate the frequency of occurrence in the 1 m s^{-1} bins. R_m is the correlation coefficient.

5 Conclusions

In the present study, an event of intense lee waves has been analyzed using the ENVISAT ASAR satellite imagery and the WRF model in the area of the Mediterranean sea localized south of Crete and Rhodos islands; this region is subject to intense and persistent low level flows, thus is favorable to the generation of atmospheric waves. Although most PBL parameterizations have demonstrated the capability to represent many meteorological phenomena, up to now little attention has been paid to the precise prediction of winds at the lowest level. Here, simulations with different diffusion and boundary layer parameterization schemes have been compared. Most of the WRF model simulations were able to forecast the existence of near-surface wind speed variability attributable to gravity waves, showing lee wave features similar to those emerging from the ASAR-retrieved wind field and interference patterns between the waves generated by different islands. The simulations with the YSU scheme and

no diffusion is the closest to the ASAR data both qualitatively and quantitatively. In order to conclude that the configuration with the YSU scheme is the best for wind field simulation, it is proposed, in the future, to compare the simulations also with other types of observations (buoys, surface stations, . . .) and in different atmospheric conditions.

The analysis of further cases in the same area, showing other features (funnelling effects, island sheltering effects, . . .) due to the interaction of high winds with the local orography, is in progress and will be the subject of a forthcoming paper.

Acknowledgements. The Envisat ASAR Wide Swath image data have been provided by the European Space Agency (on the framework of the Project Start Up C1P.5404 of the European Space Agency). Scatterometer QuikSCAT data have been downloaded from the Physical Oceanography Distributed Active Archive Center (PODAAC) of the Jet Propulsion Laboratory, Pasadena, USA.

Edited by: A. M. Sempreviva
Reviewed by: two anonymous referees

References

Atkinson, B. W.: Meso-scale atmospheric circulations, Academic Press Ltd., London, 1981.

Dudhia, J.: Numerical study of convection observed during the Winter Monsoon Experiment using a mesoscale two-dimensional model, J. Atmos. Sci., 46, 3077–3107, 1989.

ESA: ASAR Product Handbook, European Space Agency, Paris, France, 2002.

Gibbs, J. A. and Fedorovich, E.: Sensitivity of near-surface meteorological fields in WRF to boundary/surface-layer parameterizations in conjunction with horizontal grid spacing, 10th Users' Workshop, Boulder, CO, 23–26 June, 2009.

Gjevik, B. and Marthinsen, T.: Three-dimensional lee-wave pattern, Q. J. Roy. Meteor. Soc., 104, 947–957, 1978.

Green, M.: Performance of WRF for wind energy applications over complex terrain over complex sites in New Zealand and Australia, 10th Users' Workshop, Boulder, CO, 23–26 June, 2009.

Hersbach, H., Stoffelen, A., and de Haan, S.: An improved scatterometer ocean geophysical model function: Cmod5, J. Geophys. Res., 11, 5767–5780, 2007.

Hong, S.-Y. and Pan, H. L.: Nonlocal boundary layer vertical diffusion in a medium range forecast model, Mon. Weather Rev., 124, 2322–2339, 1996.

Janjic, Z. I.: Nonsingular implementation of the MellorYamada Level 2.5 Scheme in the NCEP Meso model. National Centers for Environmental Prediction Tech. Rep. 437, 61 pp., 2001.

JPL: QuikSCAT Science Data Product User Manual: QuikSCAT science data product user manual: overview and geophysical data products, Version 3.0, September 2006, D-18053-RevA, Jet Propulsion Laboratory (JPL), California Institute of Technology, 91 pp., 2006.

Kain, J. S.: The Kain-Fritsch convective parameterization: An update, J. Appl. Meteorol., 43, 170–181, 2004.

Koletsis, I., Lagouvardos, K., Kotroni, V., and Bartzokas, A.: The interaction of northern wind flow with the complex topography of Crete Island – Part 1: Observational study, Nat. Hazards Earth Syst. Sci., 9, 1845–1855, doi:10.5194/nhess-9-1845-2009, 2009.

Loughner, C. P., Allen, D. J., Dickerson, R. R., Zhang, D.-L., Shou, Y.-X., and Pickering, K. E.: Investigating the Use of a High Resolution WRF-URBAN CANOPY Model Simulation With CMAQ, 8th Annual CMAS Conference, Chapel Hill, NC, 19–21 October, 2009.

Mlawer, E. J., Taubman, S. J., Brown, P. D., Iacono, M. J., and Clough, S. A.: Radiative transfer for inhomogeneous atmosphere: RRTM, a validated correlated-k model for the longwave, J. Geophys. Res., 102, 16663–16682, 1997.

Orlanski, I.: A rational subdivision of scales for atmospheric processes, B. Am. Meteorol. Soc., 56, 527–530, 1975.

Scorer, R. S. and Wilkinson, M.: Waves in the lee of an isolated hill, Q. J. Roy. Meteor. Soc., 82, 419-427,1956.

Skamarock, W. C., Klemp, J. B., Dudhia, J., Gill, D. O., Barker, D. M., Wang, W., and Powers, J. G.: A description of the Advanced Research WRF Version 2, NCAR Technical Note, 468STR, 88 pp., 2005.

Smagorinsky, J.: General circulation experiments with the primitive equations. Part I. The basic experiment, J. Meteorol., 14, 184–185, 1963.

Smith, R. B.: The influence of mountains on the atmosphere, Adv. Geophys., 21, 87–230, 1979.

Smith, R. B.: Hydrostatic airflow over mountains, Adv. Geophys., 31, 1-41, 1989.

Smolarkiewicz, P. K. and Rotunno, R.: Low Froude number flow past three-dimensional obstacles. Part I: Baroclinically generated lee vortices, J. Atmos. Sci., 46, 1154-1164, 1989.

Sood, A. and Bange, J.: Validating coastal, near and far offshore boundary layer parameterizations with airborne helipod turbulence probe, EMS Annual Meeting Abstracts, Vol. 6, EMS2009-372, 2009.

Thompson, G., Rasmussen, R. M., and Manning, K.: Explicit forecasts of winter precipitation using an improved bulk microphysics scheme. Part I: Description and sensitivity analysis, Mon. Weather Rev., 132, 519–544, 2004.

Thomson, R. E., Vachon, P. W., and Borstad, G. A.: Airborne synthetic aperture radar imagery of atmospheric gravity waves, J. Geophys. Res., 97, 14249–14257, 1992.

Vachon, P. W., Johannessen, O. M., and Johannessen, J. A.: An ERS 1 synthetic aperture radar image of atmospheric lee waves, J. Geophys. Res., 99, 22483–22490, 1994.

Vachon, P. W, Johannessen, J. A., and Browne, D. P.: ERS-1 images of atmospheric gravity waves, IEEE T. Geosci. Remote, 33, 1014–1025, 1995.

Van der Velde, I. R., Steeneveld, G. J., Wichers Schreurs, B. G. J., and Holtslag, A. A. M.: Modeling and forecasting the onset and duration of a severe Dutch fog event, EMS Annual Meeting Abstracts, Vol. 6, EMS2009-13, 2009.

Weisman, M., Davis, C., and Wang, W.: Explicit convective forecasting with the WRF model, WRF-MM5 Workshop, Boulder, CO, 30 June, 2005.

Zecchetto, S. and De Biasio, F.: On shape, orientation and structure of atmosheric cells inside wind rolls in two SAR images, IEEE T. Geosci. Remote, 40, 2257–2262, 2002.

Zecchetto, S. and De Biasio, F.: A Wavelet Based Technique for Sea Wind Extraction from SAR Images, IEEE T. Geosci. Remote, 46, 2983–2989, 2008.